

Hot subdwarfs formed from the merger of two He white dwarfs

Josiah Schwab¹*

¹*Department of Astronomy and Astrophysics, University of California, Santa Cruz, CA 95064, USA*

5 March 2018

ABSTRACT

We perform stellar evolution calculations of the remnant of the merger of two He white dwarfs (WDs). Our initial conditions are taken from hydrodynamic simulations of double WD mergers and the viscous disc phase that follows. We evolve these objects from shortly after the merger into their core He-burning phase, when they appear as hot subdwarf stars. We use our models to quantify the amount of H that survives the merger, finding that it is difficult for $\gtrsim 10^{-4} M_{\odot}$ of H to survive, with even less being concentrated in the surface layers of the object. We also study the rotational evolution of these merger remnants. We find that mass loss over the $\sim 10^4$ yr following the merger can significantly reduce the angular momentum of these objects. As hot subdwarfs, our models have moderate surface rotation velocities of $30 - 100 \text{ km s}^{-1}$. The properties of our models are not representative of many apparently-isolated hot subdwarfs, suggesting that those objects may form via other channels or that our modelling is incomplete. However, a sub-population of hot subdwarfs are moderate-to-rapid rotators and/or have He-rich atmospheres. Our models help to connect the observed properties of these objects to their progenitor systems.

Key words: subdwarfs, white dwarfs, stars: abundances, stars: rotation

1 INTRODUCTION

The hot subdwarf stars (of spectral types O and B) are He-burning stars with H envelopes too small ($\lesssim 10^{-2} M_{\odot}$) to support H shell-burning; see Heber (2009) and Heber (2016) for recent reviews of these objects. (Hereafter, we use sdOB as a generic shorthand for hot subdwarf stars, rather than as an indicator for any particular sub-population.) Many sdOB stars are found in binary systems, where interaction has previously stripped the H-envelope. However, some sdOB stars are observed to be presently single. As described by Webbink (1984), the merger of two He white dwarfs (WDs) provides a natural mechanism for producing these objects. In such a scenario, most of the H was ejected during the earlier binary evolution that formed the tight double He WD binary and then the merger itself causes the ignition of He burning. After a phase of adjustment, the object settles into a core He-burning (CHeB) configuration.

Iben & Tutukov (1986) discuss this scenario in more detail and qualitatively consider several properties of the merged objects. They suggest that the H layers initially present on the He WDs will be buried by the turbulent mixing that occurs during the merger. Much of the H may be

consumed, though diffusion may return some to the surface. They also discuss the rotation of these objects and speculate that even if a significant fraction of the pre-merger orbital angular momentum is retained by the remnant, this could be extracted by magnetic stellar winds such that the final object might not be rapidly rotating.

Iben (1990) constructs quantitative models of He WD mergers, treating the merger as a super-Eddington accretion event. These models ignite He off-center and this He burning migrates inwards through a series of flashes. It reaches the center having burned only a small fraction of the total He and the object settles into a CHeB phase. Saio & Nomoto (1998) construct similar models using lower, sub-Eddington accretion rates and find similar results. Together, these studies confirm the basic idea of merger-initiated He ignition.

Saio & Jeffery (2000) further demonstrate that stellar models during the phase where He-burning is migrating inwards are in agreement with the observed properties of some extreme He stars. Their interpretation is that objects such as V652 Her are the result of He WD mergers and that they will subsequently evolve to be sdOB stars. Population synthesis studies of the formation of sdOB stars indicate that the He WD merger channel can indeed play a significant role in the formation of single sdOB stars (Han et al. 2002, 2003; Han 2008).

* Hubble Fellow; E-mail: jwschwab@ucsc.edu

Recent work had improved the modelling of double He WD merger remnants and more quantitatively compares the model properties to observations. [Zhang & Jeffery \(2012a\)](#) build models that approximate the merger as a mix of fast and slow accretion. Their models have surface temperatures, gravities, and abundances (in particular N and C) in agreement with the observed population of He-sdO stars. [Hall & Jeffery \(2016\)](#) address the important question of how much H can survive the merger. They show that models with their estimated surviving H masses are in agreement with the atmospheric properties of the observed population of apparently-isolated, H-rich sdB stars.

Most studies of the remnants of double WD mergers (including the aforementioned ones) circumvent the complicated hydrodynamic processes of the WD merger and its aftermath by treating this as an accretion phase. Such models are relatively simple to construct and provide valuable insights. However, these approaches can make it difficult to address questions related to the unmodeled material in the “accretion reservoir”, such as the evolution of its chemical composition or angular momentum.

Numerical hydrodynamics has long been used to study double WDs that undergo dynamically unstable mass transfer (e.g., [Benz et al. 1990](#)). Such calculations show that the system reaches a configuration with the relatively undisturbed primary WD surrounded by the tidally-disrupted secondary WD. The latter consists of an envelope of shock-heated material and a rotationally-supported disc.

[Shen et al. \(2012\)](#) show that the remnant disc, which is unstable to the magneto-rotational instability, evolves viscously on a timescale of ~hours (see also [van Kerkwijk et al. 2010](#)). [Schwab et al. \(2012\)](#) follow the evolution of these viscous discs using multidimensional hydrodynamics calculations that include an appropriate equation of state and an α -viscosity. Together, these papers show that the remnants evolve towards a spherical end-state, where the rotationally-supported disc has been converted into a hot, thermally-supported envelope.

This understanding suggests the limitations of modelling the long-term evolution as the accretion of the low mass WD onto the massive WD. Instead, the post-merger evolution is a stellar evolution problem driven by the internal redistribution of heat and momentum and not by the external accretion of mass. Motivated by that understanding, this work takes initial conditions from [Schwab et al. \(2012\)](#) and maps these into the MESA stellar evolution code. We then evolve the models forward to the CHeB phase (when they become sdOB-like) and characterize their properties.

There are two primary questions that we seek to address with these models: (1) how much hydrogen can survive the merger and later reach the surface and (2) how much angular momentum can be shed as the remnants evolve. Already [Iben & Tutukov \(1986\)](#) discuss both of these questions qualitatively; decades later, we seek to address them more quantitatively.

In Section 2 we describe the initial conditions for our models and in Section 3 show how they evolve towards a CHeB phase and beyond. In Section 4 we address the question of how much H can survive this evolution; in Section 5 we discuss the rotation of these objects. In Section 6, we summarize and conclude.

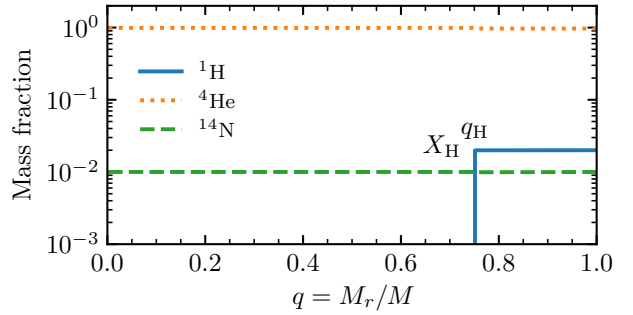


Figure 1. Parameterized composition used in the initial MESA models. We include a mass fraction X_{H} of ^1H in the outer layers (above normalized mass coordinate q_{H}) and a constant mass fraction of 0.01 ^{14}N throughout. The remaining material is ^4He .

2 INITIAL CONDITIONS AND MODELLING ASSUMPTIONS

We use release 10108 of MESA (Modules for Experiments in Stellar Astrophysics; [Paxton et al. 2011, 2013, 2015, 2018](#)) to evolve our stellar models. The input files necessary to reproduce our results will be made available at <http://mesastar.org>. For detailed descriptions of specific options, consult the MESA website at <http://mesa.sourceforge.net> and the MESA instrument papers.

2.1 Initial Conditions

Our fiducial model is the result of an $0.2 M_{\odot} + 0.3 M_{\odot}$ WD merger (model M05). We also consider a $0.3 M_{\odot} + 0.4 M_{\odot}$ WD merger model (model M07). The smoothed particle hydrodynamics (SPH) calculations of the merger are from [Dan et al. \(2011\)](#) and the post-merger viscous evolution of these systems was performed in [Schwab et al. \(2012\)](#).

Following a similar procedure to [Schwab et al. \(2016\)](#), we reduce the output of the multidimensional viscous evolution simulations to 1D profiles. The viscous evolution was performed with a grid-based code in spherical coordinates assuming azimuthal symmetry. Thus, we first calculate the total mass, internal energy, and angular momentum of the zones in each spherical shell. Then, we use these values and the equation of state (the HELM EOS, [Timmer & Swesty 2000](#)) to produce profiles of the average density, temperature and specific angular momentum corresponding to each spherical radius. A similar procedure also gives composition profiles; however, these are essentially pure He because the H layers that would be present on the He WDs were not included in the SPH simulations of the WD mergers and little He burning took place during the merger and subsequent viscous evolution.

Since we are interested in exploring the fate of the H, we must make an ad hoc assumption about where the H is located after the merger. We initialize our models with a uniform ^1H mass fraction X_{H} in the outer layers (those above a normalized mass coordinate q_{H}). We use this to make the assumption that turbulent mixing during the merger and its aftermath uniformly mixed the initial H throughout the tidally disrupted secondary WD and perhaps destroyed H in

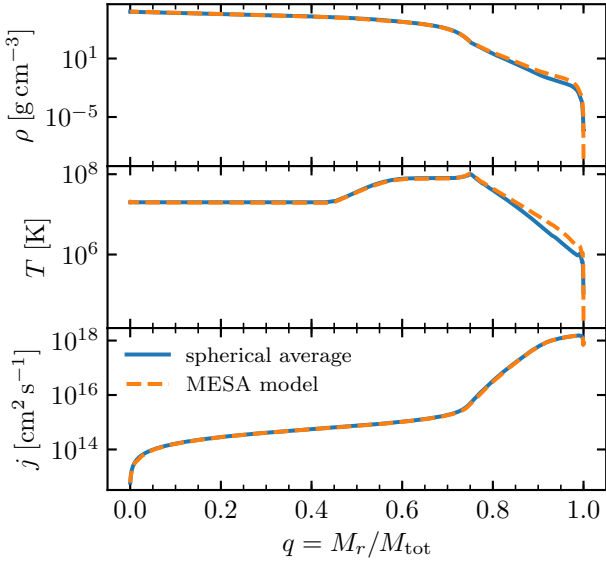


Figure 2. Comparison of density, temperature, and specific angular momentum profiles between spherical averages taken at the end of the hydrodynamic calculations of the viscous disc phase and the initial MESA model for our fiducial model M05.

the inner regions. In Section 4 we will motivate and discuss our choices of X_{H} and q_{H} and also demonstrate that our results are not sensitive to their precise values. We also assume the material is roughly solar metallicity and put a uniform abundance of 1 per cent by mass of ^{14}N . This is of particular importance, since the H will primarily be destroyed via the CNO cycle. Figure 1 illustrates this schematic composition profile. We use the MESA default 8 isotope nuclear network `basic.net` which covers H and He burning.

We use the built-in MESA `relax_initial` controls to construct a MESA model with the given density, temperature and composition profiles. These relaxation routines construct MESA models that match given input profiles by evolving an arbitrary initial model with an extra heating term, extra torque term, or extra composition change term. These extra terms are chosen such that they guide the model towards the desired structure on a relaxation timescale that is short compared to other characteristic timescales in the model. This proceeds for a large number of relaxation timescales such that the structure of the MESA model becomes close to the input profiles. (A exact match may not be possible given that the input profiles may not satisfy the equations solved by MESA.) Figure 2 shows that the input spherical average profiles are approximately realized in the MESA model. Some differences do appear in the outer layers ($q \gtrsim 0.75$) reflecting departures from spherical symmetry and hydrostatic equilibrium in these regions. We then load these models into MESA and evolve them forward in time.

2.2 Modelling Assumptions

Our fiducial model does not include element diffusion in order to reduce its computational cost. However, we do run models including element diffusion. By virtue of using a re-

cent MESA release, this takes advantage of improvements of the treatment of diffusion in degenerate regions (see section 3 in Paxton et al. 2018).

Beginning from the initial angular momentum profile given by the viscous evolution calculations, our models continue to approximately include the effects of rotation. MESA treats rotation in the shellular approximation (see section 6 in Paxton et al. 2013). The angular momentum transport and rotationally-induced mixing is performed in a diffusive framework as in Heger et al. (2000). We include the processes of Eddington-Sweet circulation, the Goldreich-Schubert-Fricke instability, the Solberg-Høiland instability, the secular shear instability, and the Spruit-Tayler dynamo. The rotational corrections to the stellar structure equations are included via the factors f_{T} and f_{p} (Endal & Sofia 1976). Note that these values have enforced minimum limits that are triggered if the outer layers approach critical rotation. As we will show in Section 5, material often reaches or exceeds critical rotation. The results from 1D calculations are necessarily particularly uncertain in this regime. Nonetheless, this represents a first effort towards quantitatively characterizing the role of rotation.

As is well-known, the duration of the CHeB phase depends on the mixing processes that set the size of the convective core (e.g., Salaris & Cassisi 2017). The work of Schindler et al. (2015) explores many of the important choices related to this issue when making MESA models of sdB stars. We use the OPAL C- and O-enhanced (“Type II”) opacities (Iglesias & Rogers 1996). We adopt mixing parameters from Paxton et al. (2018) that make use of the improved treatment of convective boundaries described in that work. We do not include additional processes such as convective overshoot that might further extend the core. We do not attempt to tune the mixing parameters to match asteroseismic constraints on the convective core size (Van Grootel et al. 2010b,a; Charpinet et al. 2011), as that is beyond the scope of this work.

3 SCHEMATIC EVOLUTION

Before we discuss our models in more detail, we briefly demonstrate their evolution from the immediate post-merger state to the CHeB phase. Figure 3 shows this evolution for the fiducial model M05. The signature of the first $\sim 10^2$ yr of the evolution is driven by the initial properties of the outer layers. These are the least spherical, most rotationally supported regions at the end of the viscous calculations. Thus, they are the most uncertain regions in our MESA modelling (see also Figure 10 and surrounding discussion). We do not focus on the details of this early evolution.

Beginning around $\sim 10^2$ yr and continuing for $\sim 10^3$ yr, the remnant expands as it thermally adjusts. This is followed by a $\sim 10^4$ yr phase in which the remnant radiates away much of the thermal energy deposited during the merger.¹ As their thermal support is lost, the non-degenerate outer layers Kelvin-Helmholtz contract, eventually leading to He ignition near their base. (The M07 model is similar, though

¹ To clearly demonstrate that the energy radiated is that deposited in the merger, the M05 model we show in Figure 3 has no H, and so has negligible nuclear energy release before 10^4 yr.

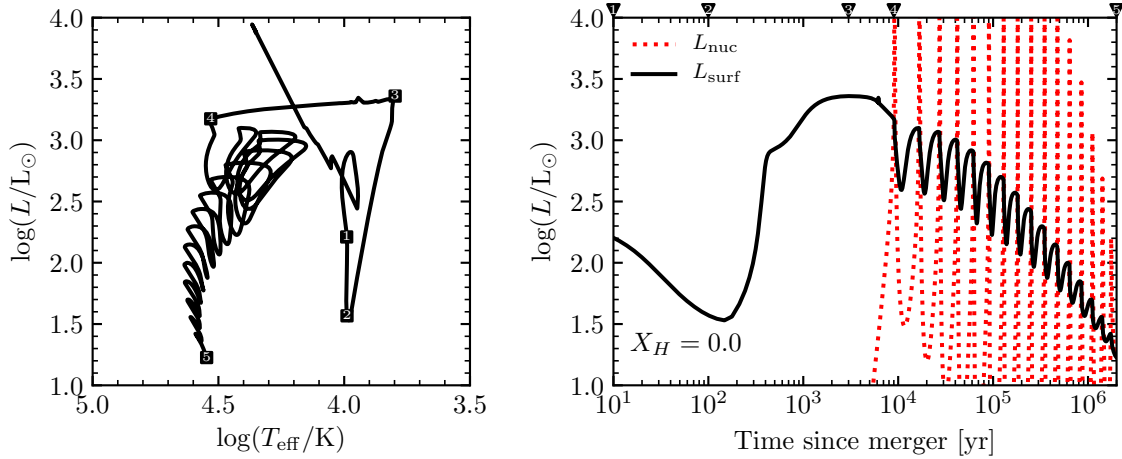


Figure 3. Evolution of the M05 model up to the onset of the CHeB phase. The left panel shows the HR diagram. The right panel shows the luminosity as a function of time. There, the solid line shows the surface luminosity; the dashed line shows the nuclear luminosity. This model has no H, so the nuclear energy release is from He burning. The shared y-axis gives a correspondence between the two panels; as an aid, numbered squares are placed on the left track at the times marked by numbered triangles at the top of the right panel.

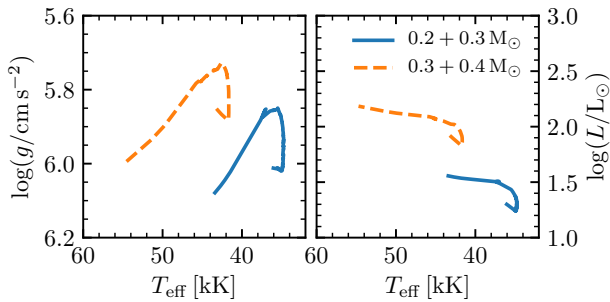


Figure 4. Location of the models on the Kiel diagram (left) and HR diagram (right) during their He core burning phase. The models shown have essentially no H envelope.

the higher primary WD mass means that He burning begins almost immediately.) Once He burning is ignited off-center there is a $\sim 10^6$ yr phase during which the He burning migrates to the center through a series of flashes. This is in agreement with the results of previous work (Iben 1990; Saio & Nomoto 1998). The object then enters a long-lived ($\sim 10^8$ yr) CHeB phase. Figure 4 shows the surface gravity, effective temperature, and luminosity of our models during this phase.

After the CHeB phase, there is an off-center He shell-burning phase of duration $\sim 10^7$ yr. Like the results of Zhang & Jeffery (2012a), our $0.5 M_{\odot}$ and $0.7 M_{\odot}$ models do not experience a cool giant phase (where they would appear like R Coronae Borealis stars) during shell burning; only a more massive $\approx 0.8 M_{\odot}$ model would have such a phase (Zhang & Jeffery 2012b). Once He shell burning ends, the object moves towards the WD cooling track. Some of our models experience brief He flashes before finally moving down the cooling track. If significant H survives and is brought to the surface by diffusion, the models have the H atmospheres of DA WDs; otherwise, they have the He atmospheres of DB WDs.

4 HYDROGEN

We wish to understand the surface H abundance of the WD merger remnants during the phase when they appear as sdOB stars. This observable will be affected by nuclear burning, which decreases the total amount of H, and by element diffusion, which serves to move the surviving H towards the surface. We do not confront the full richness of the observational data with our models, instead choosing to initially focus on the simpler questions of how much H survives and concentrates at the surface.

Within the hot subdwarf population, there is significant diversity of the surface H and He abundances. Most sdB stars have H-rich surfaces with a population-average He/H number ratio ≈ 0.01 .² Asteroseismic analyses of pulsating sdB stars (e.g., Brassard et al. 2001) allow measurement of the fractional mass of the outer H-rich envelope; the compilation of Fontaine et al. (2012) lists measured values for sdBs roughly in the range $-5.0 \lesssim \log(M_{\text{env}}/M) \lesssim -2.5$. There is also a rare population of sdB stars with He-dominated surfaces (He-sdB; Green et al. 1986; Ahmad & Jeffery 2003; Naslim et al. 2010). The sdO stars have both He-deficient and He-enriched sub-classes (e.g., Hirsch et al. 2008). Fully successful models of sdOB stars should, for example, reproduce the correlation between effective temperature and He abundance (Edelmann et al. 2003).

4.1 Destruction via H burning

Hydrogen is not included in the SPH simulations of the double WD mergers that we use (Dan et al. 2011), but in reality

² While low (i.e., sub-solar), such values are in fact puzzlingly high. If diffusion were allowed to operate unimpeded, the surface layers would become essentially pure H on a timescale much shorter than the CHeB lifetime. This issue and possible resolutions, such as mass loss or additional turbulent mixing, have been discussed by Michaud et al. (2011) and Hu et al. (2011).

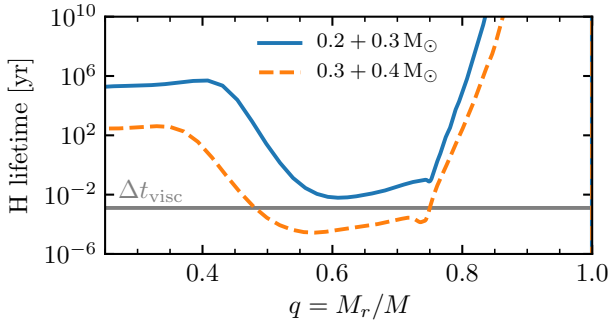


Figure 5. Timescale for H destruction in the initial MESA models. The horizontal grey line shows the duration of the viscous phase simulations.

low mass He WDs have thick H envelopes. Since we cannot include H self-consistently, we instead make the simple choice to adopt an initial condition with a uniform distribution of H in the outer layers (see Section 2). Physically, this corresponds to the assumption that turbulent mixing redistributes all the H within these regions.

Hall & Jeffery (2016) use stellar evolution calculations to characterize the mass of H expected in the envelopes of the two He WDs at merger. Across the range of He WD masses and ages they find the H layer mass is typically $3 \times 10^{-4} - 3 \times 10^{-3} M_{\odot}$. Modelling the merger as a “cold” accretion process in which none of this H is destroyed then gives an upper limit on the amount of H that can be present in the merged remnant. However, one expects that some of that H will be destroyed by the high temperatures during and after the merger. Dan et al. (2014) use the results of a suite of SPH simulations to provide fitting formulae that give the fractional mass in each of the components (core, envelope, and disc) of the merged remnant. Hall & Jeffery (2016) assume that the H present at merger is distributed uniformly through the disc and envelope by turbulent mixing and then assume complete H destruction in the hot envelope. Since the disc and envelope components have comparable masses, the surviving H mass is typically less than the initial H mass by a factor of ≈ 2 . As Hall & Jeffery (2016) discuss, this is still an upper limit to the amount of surviving H. Modelling the post-merger pre-CHeB phase, as our work does, is necessary to address further H destruction.

Figure 5 shows the timescale for H destruction in the initial conditions of our models. The length of the viscous simulation was 4×10^4 s and is marked by the horizontal grey line. Around the broad temperature peak ($q \approx 0.6$), H would be destroyed during the viscous phase or shortly thereafter. The timescale in the outer layers is much longer; this motivates our fiducial choice of $q_{\text{H}} = 0.75$. We also adopt a fiducial abundance $X_{\text{H}} = 0.01$ as this gives total H masses $\sim 10^{-3} M_{\odot}$, of order the expected amount (see e.g., figure 12 in Istrate et al. 2016).

The upper panel of Figure 6 shows the temperature profile of the fiducial model M05 at a sequence of times during its evolution towards the CHeB phase. The inward-moving He-burning front is apparent in the left of the plot. The structure of the outer layers evolves such that only a small amount of mass is at temperatures $\lesssim 10^7$ K. The lower panel

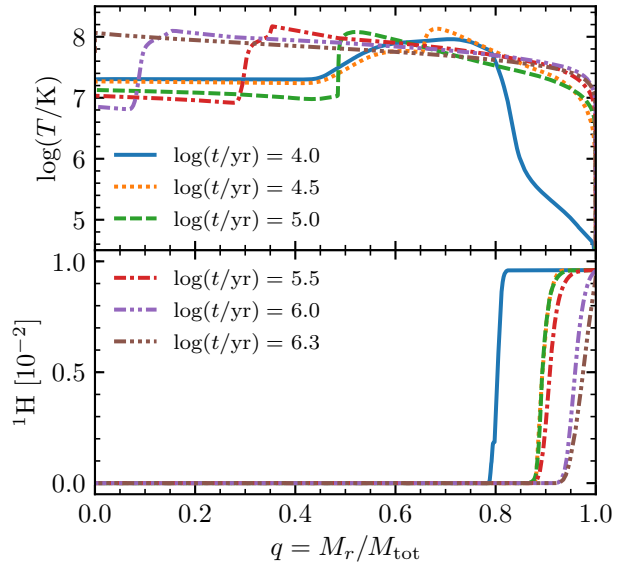


Figure 6. Temperature (upper panel) and H mass fraction (lower panel) profiles at the indicated times in model M05. This model does not include the effects of element diffusion.

shows the profile of the H mass fraction; most H internal to $q \approx 0.95$ is destroyed.

It is a robust feature of our models that H is destroyed throughout a significant fraction of the material that was originally part of the disc component. As such, the surviving hydrogen masses in our models are much less than those in Hall & Jeffery (2016). In contrast to their models in which approximately half of the H survives post-merger, our models typically have only roughly a tenth of the initial H remaining. Figure 7 shows the mass of surviving H. Since H is always destroyed within the inner regions ($q \lesssim 0.95$), the mass of surviving H displays little dependence on its initial distribution. In all cases shown in Figure 7 the surviving H mass is $\approx 10^{-4} M_{\odot}$. The more massive model M07 also has surviving H masses $\approx 10^{-4} M_{\odot}$. With the assumption of uniform mixing, the absolute mass of surviving H necessarily depends on the initial mass, since the H present in the outermost layers will survive. In our models, at fixed q_{H} , a higher value of X_{H} leads to a larger surviving H mass. However, for our fiducial value of $q_{\text{H}} = 0.75$, varying the initial value of X_{H} by a factor of two in each direction left the percentage of the initial H that survived essentially unchanged at ≈ 10 per cent.

While H destruction comes naturally from our modelling of the post-merger phase, we emphasize that this finding is not unique to our approach. This same qualitative result can be reproduced in simulations that model the merger as an accretion event. To demonstrate this, we begin with a $0.3 M_{\odot}$ He WD (without a pre-existing H envelope) and accrete material with $X_{\text{H}} = 0.01$ at a rate $2 \times 10^{-6} M_{\odot} \text{ yr}^{-1}$ until the object reaches a mass of $0.5 M_{\odot}$. The object ignites off-center He burning, but the final total mass is reached before the He burning reaches the center. As newly-accreted material is compressed, it reaches temperatures where the H burns; subsequently, after accretion ceases, H destruction

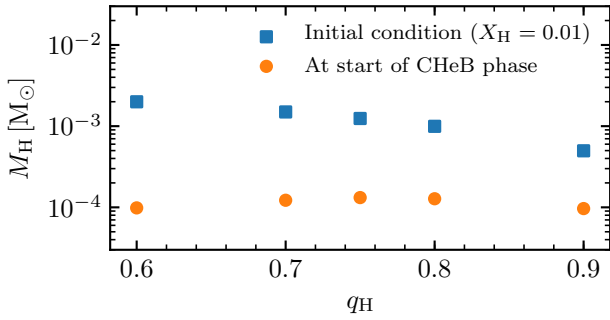


Figure 7. Mass of H surviving at the time model M05 reaches the CHeB phase. The parameter on the x-axis, q_H , indicates different choices for the initial extent of the H.

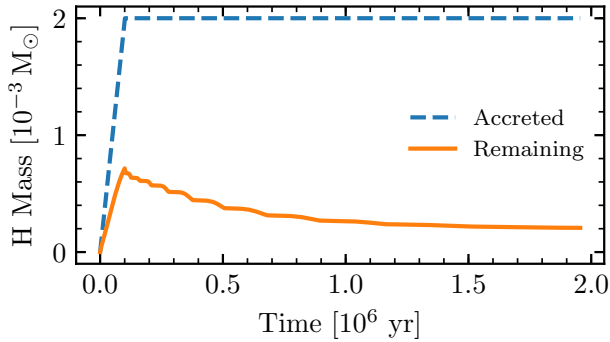


Figure 8. Evolution of an “accretion” model similar to our fiducial model (see text). The dashed line shows the cumulative accreted mass of H; the solid line shows the surviving H mass. The calculation stops when the model reaches the CHeB phase.

continues as additional time elapses and the object’s structure adjusts. Figure 8 shows the mass of H that survives as a function of time. Most of the accreted H is destroyed and only $\approx 2 \times 10^{-4} M_\odot$ survives when the model reaches the CHeB phase.

4.2 Relocation via Element Diffusion

In the previous subsection, we showed that H was destroyed throughout most of the remnant except in the outer layers. Element diffusion concentrates the lighter H (in its predominantly He background) at the surface. In principle, this could increase the amount of H that survives the merger by concentrating it in the cooler surface layers before it has time to burn. However, we find that the action of element diffusion is not sufficiently rapid to redistribute the H and prevent its destruction. Moreover, we find that the action of rotation (via mixing and mass loss) overwhelms the effects of element diffusion during the evolution towards the CHeB phase.

To isolate the roles of element diffusion and rotational mixing, we run a suite of models with and without each of these effects. Table 1 summarizes our models and indicates the total surviving H mass and the H surface abundance in

Model	Rotation	Diffusion	$M_H [10^{-4} M_\odot]$	$X_{H,\text{surf}}$
M05	yes	no	1.32	0.01
	yes	yes	1.31	0.01
	no mixing	no	1.96	0.01
	no mixing	yes	1.96	0.03
	no	no	2.02	0.01
	no	yes	1.99	0.51
M07	yes	no	0.96	0.01

Table 1. The effects of rotation and element diffusion. The column “Rotation” indicates whether the MESA models include rotation: “yes” means rotation is included as normal, “no mixing” means the structural effects of rotation are included, but the rotational mixing coefficients are set to 0, and “no” means non-rotating models. The column “Diffusion” indicates whether element diffusion is included. The column M_H is the total surviving H mass; the column $X_{H,\text{surf}}$ is the surface H mass fraction. Both these latter quantities are given at the start of the CHeB phase.

each case (measured at the start of the CHeB phase). Models with the same rotation treatment but with and without element diffusion have nearly identical surviving H masses. This is the simple statement that the H diffusion timescale is not shorter than the H destruction timescale in the deeper layers. Given the minor effect of rotation and diffusion, we run only one version of model M07 which uses our fiducial assumptions.

Comparing models with and without rotational mixing, one sees rotational mixing causes additional H destruction, as this can mix H into deeper layers. Allowing element diffusion to operate without the interference of rotational mixing leads to a slightly higher surface H fraction. However, only the completely non-rotating model develops a surface H abundance $\gtrsim 0.1$. This reflects the fact that rotating models typically shed their outer layers (see Section 5), meaning that any surface abundance enhancement does not accumulate.

During the longer lived, higher surface gravity CHeB phase the diffusion timescale becomes short compared to the evolutionary timescale. Figure 9 shows the surface H abundance, the mass of the H-rich layer (defined as where the H mass fraction > 0.1), and the total H mass for our MESA models during the CHeB phase. These are continuations of the three M05 models with diffusion from Table 1. In cases without rotational mixing, the surface quickly becomes pure H and the H-rich layer mass grows. In the case with rotational mixing, this process overwhelms diffusion and the star does not develop an H-rich surface. In all cases, some H continues to be destroyed during the CHeB phase.

The H-rich layer masses that develop when diffusion operates unimpeded are $\lesssim 10^{-5} M_\odot$, even at the end of the CHeB phase. In the compilation of [Fontaine et al. \(2012\)](#), several apparently-single sdB stars have asteroseismically measured envelope masses in excess of this value. The work of [Hall & Jeffery \(2016\)](#) also required H masses of $\sim 10^{-3} M_\odot$ to match the atmospheric properties of the observed H-rich sdBs. It is a challenge for our merger models to explain such objects.

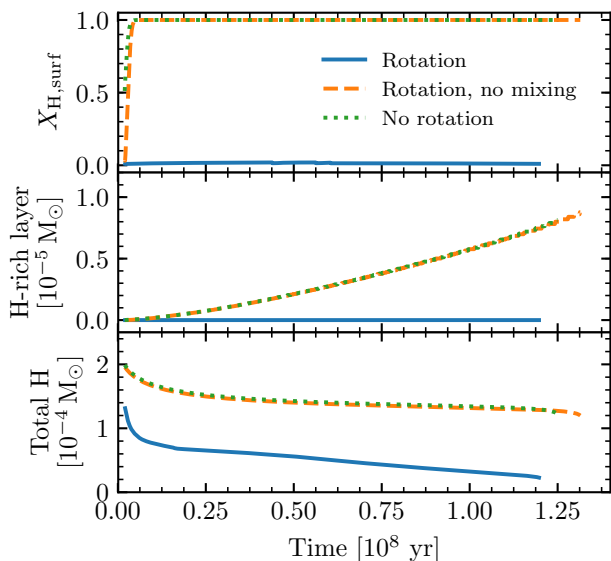


Figure 9. Surface H mass fraction (upper panel), mass in H-rich layer (middle panel), and total H mass (lower panel) during the CHeB phase. The different lines show runs of model M05 with different treatments of rotation and its effects; all models have element diffusion.

5 ROTATION

The previous section briefly discussed rotation as a cause of additional mixing. Here, we wish to understand the rotation rate of the WD merger remnants during the phase when they appear as sdOB stars. The merged system initially retains much of the orbital angular momentum of the binary. As discussed by Gourgouliatos & Jeffery (2006), if the evolution were strictly conservative, that amount of angular momentum would cause the star to be rotating in excess of critical rotation when it reached the CHeB phase. During the viscous evolution, angular momentum is transported outwards, but in the calculations of Schwab et al. (2012) significant mass and angular momentum were not lost from the system. Thus, in our initial conditions, the remnant still has a total angular momentum that exceeds that of a critically-rotating CHeB star of the same mass.

Figure 10 shows the initial rotation profile (as a fraction of critical rotation) for our fiducial model along with the same quantity from the spherical average of the viscous simulation. These quantities are not the same, reflecting differences in the structure of the outer layers that occur when mapping from multi-D to 1D (see Figure 2). More sophisticated averaging, such as averaging along isobars instead of spherical shells, might somewhat improve the level of agreement, but we do not explore this here. The quantity of primary interest, the total angular momentum, is the same to within less than 1 per cent.

The fact that material can be above critical rotation in the MESA model reflects the fact that the rotational corrections to the equations MESA is solving are limited (see discussion in Section 2). Numerically, this allows for material in MESA to approach or exceed critical rotation while remaining bound; physically, we know the behaviour

of this material is being poorly modelled. This caveat means that the detailed behaviour of the outer layers during the early phase of evolution is unlikely to be accurate. However, we argue that the overall picture that develops is robust against these uncertainties.

These super-critically rotating outer layers serve as an initial angular momentum reservoir. The remnant soon expands as it adjusts towards thermal equilibrium, and since the radius has increased significantly, this material quickly becomes sub-critical. Even if the configuration of the outer layers were different than in our initial MESA model, we would still expect it to eventually realize a similar configuration. For example, if some of the high-angular momentum material were instead in a rotationally-supported disc, it would be quickly engulfed as the star expands and that angular momentum incorporated in the outer layers. None of our arguments rely on the details of the behaviour during this initial $\sim 10^3$ yr expansion phase.

After realizing its extended state, the remnant begins to contract as the outer layers cool. As this occurs, the outer layers again approach critical rotation. We allow this mass to be shed from the star. The details of this process are uncertain, so we demonstrate that three mass loss prescriptions all yield similar results.

First, our default approach is to apply the Reimers mass loss rate, with a scaling factor of 0.1 (Reimers 1975). This prescription, which is intended for red giants, is merely a convenient choice for a mass loss rate that increases with increasing stellar luminosity and radius. Following Heger et al. (2000), we allow for rotationally-enhanced mass loss, scaling the mass loss rate by the factor

$$\left(1 - \frac{\Omega_{\text{surf}}}{\Omega_{\text{surf,crit}}}\right)^{-0.43}. \quad (1)$$

By default, MESA caps this enhancement factor at 10^4 .

Our second approach is to begin from the baseline of an arbitrary constant mass loss rate of $10^{-10} M_{\odot} \text{ yr}^{-1}$. Again, we allow for rotational enhancement, so the realized mass loss rate is not constant. The baseline value is chosen to be low enough that significant mass would not be lost over the $\sim 10^6$ yr evolution to the CHeB phase in the absence of rotational enhancement, but to be high enough so that the rotational enhancement factors realized in MESA lead to meaningful loss. Compared to our default choice, this approach means that mass is lost at a lower rate for a longer period. The slower mass loss means that material is not lost immediately upon reaching critical rotation and thus there is time for angular momentum to be redistributed before the mass is shed. This leads to less mass and angular momentum being lost than the other approaches.

The third approach makes use of built-in MESA capabilities that can, at each timestep, find the mass loss rate that will keep the star below critical rotation. This approach avoids invoking any particular form for the rotationally-enhanced mass loss (such as equation 1). Since the initial condition is super-critically rotating, we do not activate this mass loss until after the first 10^3 yr have elapsed. In this case, we also apply a small constant mass loss rate floor of $10^{-10} M_{\odot} \text{ yr}^{-1}$ (without rotational enhancement).

All of the aforementioned prescriptions are arbitrary and uncertain. However, the different approaches yield similar results. Figure 11 shows the evolution of the mass and angular

momentum for in calculations using these three prescriptions (labeled “Reimers”, “Constant”, and “Sub-critical”, respectively). Thus we argue that so long as the object loses mass in order to remain at-or-below critical rotation, we expect qualitatively similar behavior.

As indicated in Figure 10, the initial total angular momentum is $\approx 10^{50} \text{ g cm}^2 \text{ s}^{-1}$. If the shed mass carries the Keplerian angular momentum at the surface, then the corresponding change in angular momentum is

$$\Delta J = 2 \times 10^{49} \text{ g cm}^2 \text{ s}^{-1} \left(\frac{R}{30 R_{\odot}} \right)^{1/2} \left(\frac{M}{0.5 M_{\odot}} \right)^{1/2} \left(\frac{\Delta M}{10^{-3} M_{\odot}} \right). \quad (2)$$

The post-merger expansion of the remnant gives a long lever-arm, allowing the loss of a small amount of mass, $\Delta M \sim 5 \times 10^{-3} M_{\odot}$, to carry away almost all of the angular momentum.

The results in Figure 11 indicate that the amount of angular momentum retained in the remnant is $\approx 10^{48} \text{ g cm}^2 \text{ s}^{-1}$. For an $\approx 0.5 M_{\odot}$ CHeB star, the radius is $\approx 0.1 R_{\odot}$ and moment of inertia is $\approx 4 \times 10^{51} \text{ g cm}^2$. This corresponds to a surface rotation velocity of

$$v_{\text{rot}} \approx 20 \text{ km s}^{-1} \left(\frac{J}{10^{48} \text{ g cm}^2 \text{ s}^{-1}} \right) \quad (3)$$

Thus, when the MESA models reach the CHeB phase, the remnant is no longer rapidly rotating, with $v_{\text{rot}} \approx 30 \text{ km s}^{-1}$ for our fiducial model M05.

When we apply the same methods to the model M07, we find that the initial angular momentum of $\approx 2 \times 10^{50} \text{ g cm}^2 \text{ s}^{-1}$ is reduced to $\approx 10^{49} \text{ g cm}^2 \text{ s}^{-1}$ via the shedding of $\approx 0.01 M_{\odot}$. Note that the larger amount angular momentum retained in this case gives a surface rotation velocity $v_{\text{rot}} \approx 100 \text{ km s}^{-1}$.

Observationally, hot subdwarfs—including the apparently-single ones—are not fast rotators, with most objects having $v \sin i < 10 \text{ km s}^{-1}$ (Geier & Heber 2012). Thus, our models are still significantly faster rotators than most of the observed population. To further reduce the spin, potentially bringing it in closer accordance with observed values, we would require additional angular momentum to be shed during post-merger phase or in the early stages of the CHeB phase.

Angular momentum loss via magnetized stellar winds is a potentially important process that is not included in our models. Such winds are known to be important in the evolution of the rotation rates of main sequence stars and in the binary evolution of cataclysmic variables (e.g., Weber & Davis 1967; Mestel 1968; Verbunt & Zwaan 1981). Their possible importance in this context was already speculated by Iben & Tutukov (1986). The magnetic field of the remnant is likely amplified via dynamo action during the merger (Tout et al. 2008; Beloborodov 2014). Magnetohydrodynamics simulations have found fields in excess of 10^8 G in mergers of two CO WDs (Ji et al. 2013; Zhu et al. 2015). Determining the field strengths and geometries generated by WD mergers, including these lower mass He WD systems, will be an interesting path for future work.

Additionally, Geier & Heber (2012) cites an as-yet-unpublished suggestion by Ph. Podsiadlowski that angular momentum is shed during the post-merger He-flashing phase. In our models, essentially all the angular momentum loss has already occurred by the time He-flashing commences, so such a process would represent further loss.

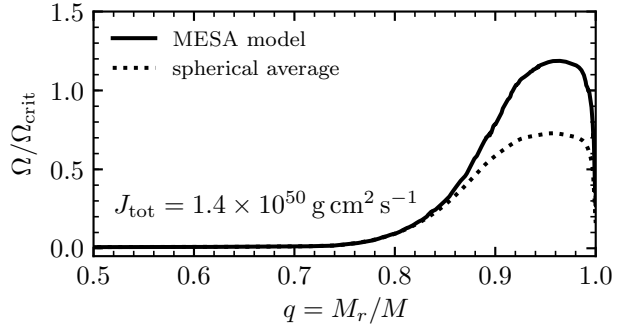


Figure 10. Rotation profile (as a fraction of critical rotation) for the initial model M05. Roughly the outer 10 per cent of material is initially super-critical.

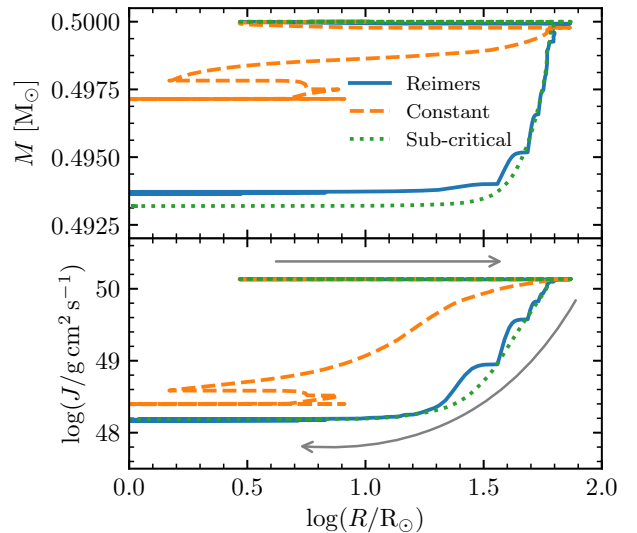


Figure 11. Evolution of the total mass and angular momentum of the fiducial model M05 versus its radius. The grey arrows in the lower panel indicate the direction of the evolution. First, there is an expanding phase; this is followed by a contracting phase, during which the outer layers reach critical rotation and mass and angular momentum are shed. The three lines correspond to the three different mass loss prescriptions described in the text.

6 SUMMARY AND CONCLUSIONS

We perform stellar evolution calculations of the remnant of the merger of two He WDs. We evolve these objects from shortly after the merger into their core He-burning phase. At this point the objects appear as hot subdwarf stars and we follow them until they form WDs. One of the key aspects of our work is that we use initial conditions motivated by hydrodynamic simulations of double WD mergers and the viscous disc phase that follows.

These initial conditions allow us to capture a phase of expansion driven by the thermal energy deposited in the remnant during the merger. As the energy is radiated away, the star subsequently contracts. At that point, the outer layers of the star reach critical rotation. We show, via rotating

stellar models, that because of the large stellar radius at this time, a small amount of mass shedding significantly reduces the total angular momentum of the remnant. Our merger model that gives a roughly canonical mass ($\approx 0.5 M_{\odot}$) hot subdwarf is rotating with $v_{\text{rot}} \approx 30 \text{ km s}^{-1}$; the more massive $\approx 0.7 M_{\odot}$ merger remnant is a more rapidly rotating object with $v_{\text{rot}} \approx 100 \text{ km s}^{-1}$. While these results demonstrate that the sdOB star remnants of WD mergers need not be rotating near breakup, they do not yield slowly rotating models in agreement with most observed objects. This may indicate the presence of other efficient angular momentum loss mechanisms not considered in this work; or it may be evidence that the slowly rotating apparently-single sdOB stars were not formed through double WD mergers. More work is needed to understand whether the trend seen in these two models implies a mass-rotation relationship, in which higher mass merger remnants should be faster-rotating.

We also study the ability of H to survive the post-merger evolution. Calculations of the merger and its aftermath do not include H, so we adopt a simple initial chemical profile. We show that if the H is uniformly distributed in the disc and envelope components of the merger, it is mostly destroyed. Beginning with initial H masses of $\sim 10^{-3} M_{\odot}$ we find surviving H masses $\approx 10^{-4} M_{\odot}$ for both our $0.5 M_{\odot}$ and $0.7 M_{\odot}$ models. This is independent of our assumptions about rotation and element diffusion. We also show that simple accretion models give a similar result. Moreover, we show that element diffusion is able to concentrate only a fraction of that H on the surface over the CHeB lifetime. At face value, this implies sdOB stars with H layer masses $\gtrsim 10^{-4} M_{\odot}$ cannot be formed via WD mergers. One way around this would be to have the H be distributed differently than our assumption (i.e., already concentrated at the surface). Future numerical WD merger calculations including H may be able to clarify the validity of our assumption about the initial H distribution.

The initial H layer masses we use are motivated by those found on He WDs from stellar evolution calculations (Hall & Jeffery 2016; Istrate et al. 2016). Note that during the gravitational-wave-driven inspiral of a He WD binary, the first mass transferred is necessarily H. This mass transfer and accompanying novae may have important consequences on the pre-merger orbital evolution of the system (e.g., D’Antona et al. 2006; Kaplan et al. 2012; Shen 2015). Burning of the transferred mass during this phase can also reduce the amount of H that is present when the merger occurs, making it even more difficult to produce remnant with a significant H layer. These issues further motivate the careful inclusion of the H envelopes in future work on these binaries.

In a picture where double He WD mergers produce most single hot subdwarfs, it is challenging to understand why the mass and rotation distributions look similar for sdB stars with and without observed companions (Geier & Heber 2012; Fontaine et al. 2012). Our results do not alleviate this tension; our models are neither slowly-rotating nor do they have H envelopes as massive as many of those reported in the compilation of Fontaine et al. (2012). The models of merger-produced hot subdwarfs in this work bear a greater resemblance to the He-sdO stars in their rotation rates and abundances (e.g., Hirsch 2009).

The accretion-based double WD merger models of

Zhang & Jeffery (2012a) successfully reproduce distributions of the surface C and N abundances observed in the He-sdO stars. We note that their models generally have relatively deep convection zones that reach the surface during the accretion phase (see their figures 13 and 14). Our models do not exhibit such convection zones, though our rotating models do have rotationally-induced mixing processes operating in the outer layers. This suggests that our models likely have different mixing properties than theirs, but our parameterized composition profiles limit our ability to make specific abundance comparisons. We note that our $0.5 M_{\odot}$ model has a mass fraction $\lesssim 10^{-3}$ of ^{12}C at the surface, while our $0.7 M_{\odot}$ model has ^{12}C surface mass fraction ≈ 0.01 . Both models retain surface ^{14}N mass fractions around their initial value. Future work will be necessary to characterize the detailed surface composition predicted from WD merger models. Coupled with a better understanding of the mass-dependence of rotation, future models can confront observations such as the finding of Hirsch (2009) that sdO stars with higher carbon abundances have higher projected rotational velocities.

ACKNOWLEDGEMENTS

We thank Ken Shen for helpful conversations, encouragement, and comments on the manuscript. We thank Marius Dan and Drew Clausen for useful discussions and acknowledge their involvement during early phases of this work. We thank the referee, Zhanwen Han, for his helpful comments. We thank the participants of the 7th and 8th meetings on Hot Subdwarfs and Related Objects for stimulating discussions and Uli Heber for his excellent review articles. We thank Pablo Marchant for his work developing the MESA initial model relaxation routines. We thank the Los Gatos Public Library, where much of this work was performed. This work made use of the Hyades computing resource supported by NSF AST-1229745. Support for this work was provided by NASA through Hubble Fellowship grant # HST-HF2-51382.001-A awarded by the Space Telescope Science Institute, which is operated by the Association of Universities for Research in Astronomy, Inc., for NASA, under contract NAS5-26555. This research has made use of NASA’s Astrophysics Data System. The plotting and analysis was enabled by `matplotlib` (Hunter 2007), `NumPy` (van der Walt et al. 2011), `ipython/jupyter` (Pérez & Granger 2007; Kluyver et al. 2016), `MesaScript` (Wolf et al. 2017), and `py_mesa_reader` (Wolf & Schwab 2017).

REFERENCES

- Ahmad A., Jeffery C. S., 2003, *A&A*, 402, 335
- Beloborodov A. M., 2014, *MNRAS*, 438, 169
- Benz W., Cameron A. G. W., Press W. H., Bowers R. L., 1990, *ApJ*, 348, 647
- Brassard P., Fontaine G., Billères M., Charpinet S., Liebert J., Saffer R. A., 2001, *ApJ*, 563, 1013
- Charpinet S., et al., 2011, *A&A*, 530, A3
- D’Antona F., Ventura P., Burderi L., Teodorescu A., 2006, *ApJ*, 653, 1429
- Dan M., Rosswog S., Guillochon J., Ramirez-Ruiz E., 2011, *ApJ*, 737, 89

- Dan M., Rosswog S., Brüggem M., Podsiadlowski P., 2014, *MNRAS*, **438**, 14
- Edelmann H., Heber U., Hagen H.-J., Lemke M., Dreizler S., Napiwotzki R., Engels D., 2003, *A&A*, **400**, 939
- Endal A. S., Sofia S., 1976, *ApJ*, **210**, 184
- Fontaine G., Brassard P., Charpinet S., Green E. M., Randall S. K., Van Grootel V., 2012, *A&A*, **539**, A12
- Geier S., Heber U., 2012, *A&A*, **543**, A149
- Gourgouliatos K. N., Jeffery C. S., 2006, *MNRAS*, **371**, 1381
- Green R. F., Schmidt M., Liebert J., 1986, *ApJS*, **61**, 305
- Hall P. D., Jeffery C. S., 2016, *MNRAS*, **463**, 2756
- Han Z., 2008, *A&A*, **484**, L31
- Han Z., Podsiadlowski P., Maxted P. F. L., Marsh T. R., Ivanova N., 2002, *MNRAS*, **336**, 449
- Han Z., Podsiadlowski P., Maxted P. F. L., Marsh T. R., 2003, *MNRAS*, **341**, 669
- Heber U., 2009, *ARA&A*, **47**, 211
- Heber U., 2016, *PASP*, **128**, 082001
- Heger A., Langer N., Woosley S. E., 2000, *ApJ*, **528**, 368
- Hirsch H. A., 2009, PhD thesis, Friedrich-Alexander University Erlangen-Nürnberg
- Hirsch H. A., Heber U., O’Toole S. J., 2008, in Heber U., Jeffery C. S., Napiwotzki R., eds, *Astronomical Society of the Pacific Conference Series Vol. 392, Hot Subdwarf Stars and Related Objects*. p. 131
- Hu H., Tout C. A., Glebbeek E., Dupret M.-A., 2011, *MNRAS*, **418**, 195
- Hunter J. D., 2007, *Computing In Science & Engineering*, **9**, 90
- Iben Jr. I., 1990, *ApJ*, **353**, 215
- Iben Jr. I., Tutukov A. V., 1986, *ApJ*, **311**, 753
- Iglesias C. A., Rogers F. J., 1996, *ApJ*, **464**, 943
- Istrate A. G., Marchant P., Tauris T. M., Langer N., Stancliffe R. J., Grassitelli L., 2016, *A&A*, **595**, A35
- Ji S., et al., 2013, *ApJ*, **773**, 136
- Kaplan D. L., Bildsten L., Steinfadt J. D. R., 2012, *ApJ*, **758**, 64
- Kluyver T., et al., 2016, in *Positioning and Power in Academic Publishing: Players, Agents and Agendas: Proceedings of the 20th International Conference on Electronic Publishing*. p. 87
- Mestel L., 1968, *MNRAS*, **138**, 359
- Michaud G., Richer J., Richard O., 2011, *A&A*, **529**, A60
- Naslim N., Jeffery C. S., Ahmad A., Behara N. T., Şahin T., 2010, *MNRAS*, **409**, 582
- Paxton B., Bildsten L., Dotter A., Herwig F., Lesaffre P., Timmes F., 2011, *ApJS*, **192**, 3
- Paxton B., et al., 2013, *ApJS*, **208**, 4
- Paxton B., et al., 2015, *ApJS*, **220**, 15
- Paxton B., et al., 2018, *ApJS*, **234**, 34
- Pérez F., Granger B. E., 2007, *Computing in Science & Engineering*, **9**, 21
- Reimers D., 1975, *Memoires of the Societe Royale des Sciences de Liege*, **8**, 369
- Saio H., Jeffery C. S., 2000, *MNRAS*, **313**, 671
- Saio H., Nomoto K., 1998, *ApJ*, **500**, 388
- Salaris M., Cassisi S., 2017, *Royal Society Open Science*, **4**, 170192
- Schindler J.-T., Green E. M., Arnett W. D., 2015, *ApJ*, **806**, 178
- Schwab J., Shen K. J., Quataert E., Dan M., Rosswog S., 2012, *MNRAS*, **427**, 190
- Schwab J., Quataert E., Kasen D., 2016, *MNRAS*, **463**, 3461
- Shen K. J., 2015, *ApJ*, **805**, L6
- Shen K. J., Bildsten L., Kasen D., Quataert E., 2012, *ApJ*, **748**, 35
- Timmes F. X., Swesty F. D., 2000, *ApJS*, **126**, 501
- Tout C. A., Wickramasinghe D. T., Liebert J., Ferrario L., Pringle J. E., 2008, *MNRAS*, **387**, 897
- Van Grootel V., Charpinet S., Fontaine G., Green E. M., Brassard P., 2010a, *A&A*, **524**, A63
- Van Grootel V., et al., 2010b, *ApJ*, **718**, L97
- Verbunt F., Zwaan C., 1981, *A&A*, **100**, L7
- Webbink R. F., 1984, *ApJ*, **277**, 355
- Weber E. J., Davis Jr. L., 1967, *ApJ*, **148**, 217
- Wolf B., Schwab J., 2017, *wmolf/py_mesa_reader: Interact with MESA Output*, Zenodo, doi:10.5281/zenodo.826958
- Wolf B., Bauer E. B., Schwab J., 2017, *wmolf/MesaScript: A DSL for Writing MESA Inlists*, doi:10.5281/zenodo.826954, <https://doi.org/10.5281/zenodo.826954>
- Zhang X., Jeffery C. S., 2012a, *MNRAS*, **419**, 452
- Zhang X., Jeffery C. S., 2012b, *MNRAS*, **426**, L81
- Zhu C., Pakmor R., van Kerkwijk M. H., Chang P., 2015, *ApJ*, **806**, L1
- van Kerkwijk M. H., Chang P., Justham S., 2010, *ApJ*, **722**, L157
- van der Walt S., Colbert S. C., Varoquaux G., 2011, *Computing in Science Engineering*, **13**, 22

This paper has been typeset from a $\text{\TeX}/\text{\LaTeX}$ file prepared by the author.